Science Signaling
AAAS

www.sciencesignaling.org/cgi/content/full/2/65/ra15/DC1

Supplementary Materials for

Spatiotemporal Patterning During T Cell Activation Is Highly Diverse

Kentner L. Singleton, Kole T. Roybal, Yi Sun, Guo Fu, Nicholas R. J. Gascoigne, Nicolai S. C. van Oers, Christoph Wülfing*

*To whom correspondence should be addressed. E-mail: christoph.wuelfing@utsouthwestern.edu

Published 7 April 2009, *Sci. Signal.* **2**, ra15 (2009)
DOI: 10.1126/scisignal.2000199

This PDF file includes:

References

Other Supplementary Material for this manuscript includes the following:
(available at www.sciencesignaling.org/cgi/content/full/2/65/ra15/DC1)

Movies S1 to S27 (MOV format)

Supplementary Text

TCR signaling enhances its inclusion in the cSMAC signaling complex

The TCR ζ–chain, one of the components of the TCR complex, signals through three immunoreceptor tyrosine-based activation motifs (ITAMs), each of which contains two tyrosine residues. Although somewhat controversial, strong evidence supports the idea that the membrane-proximal ITAM is only phosphorylated upon full activation of the T cell (*1*). We therefore made fusions of GFP to WT TCRζ, a mutant TCRζ in which the tyrosines of all three ITAMs were changed to phenylalanines (TCRζ 1-6), or a mutant TCRζ in which only the tyrosines of the membrane-proximal ITAM were changed to phenylalanine (TCRζ 1,2). We determined the spatiotemporal patterning of all three GFP-fused constructs on a WT TCRζ background to retain proper overall spatiotemporal organization of the T cell. Relative to WT TCRζ, TCRζ 1-6 and TCRζ 1,2 were enriched in two locations that were poor in signaling intermediates, the distal pole (accumulation in > 20% of cell couples up to 2 min as compared to 1 min for WT TCRζ) and a large T cell invagination [(*2*), fig. S9] (up to 25% of cell couples as opposed to < 10% of couples for WT TCRζ) (fig. S8). This was complemented by a relative depletion at the center of the T cell-APC interface (10 to 40% of cell couples with central accumulation in the first 2 min after formation of tight cell couples as opposed to 20 to 60% of cell couples for WT TCRζ). In addition, inclusion in internal punctate clusters, likely vesicles (movie S5), at > 5 min after tight cell coupling was seen in 61% and 66% of the T cells expressing TCRζ 1,2 or TCRζ 1-6, respectively, but not with T cells expressing WT TCRζ. Together, these data suggest that TCR signaling through its ζ-chain enhanced recruitment of the TCR to the cSMAC signaling complex, establishing it as an area of active signaling, rather then leaving the TCR at the uropod, in the large T cell invagination, or in internal vesicles. Our systems-level description of the spatiotemporal patterning in T cell activation thus was critical in distinguishing signaling-active from less signaling-active locations of TCR accumulation.

Rho activity is required for the resolution of the large T cell invagination

We have recently discovered a large T cell invagination that forms immediately after formation of the T cell-APC couple (*2*). We suggested that it serves to internalize partial signaling complexes to reset the T cell signaling machinery upon formation of cell couples. To test this hypothesis, we analyzed the enrichment of receptors and signaling intermediates in the invagination. Upon T cell stimulation with professional APCs in the presence of 10 μM antigenic peptide, 25 to 35% of cell couples showed accumulation of receptors in the invagination: CD2 and CD28 in 5C.C7 T cells (fig. S9), and the TCR in DO11.10 T cells (fig. S12). Accumulation of proximal signaling intermediates, for example ZAP-70, LAT, and PKCθ, was significantly less (see fig. S9 legend) Only 10 to 20% of the cell couples showed enrichment of signaling intermediates in the invagination (fig. S9 and fig. S12) for both 5C.C7 and DO11.10 T cells. Thus, receptors in the invagination were associated with fewer signaling intermediates than were those receptors directly at the T cell-APC interface, corroborating the hypothesis that the large T cell invagination may serve to internalize partial signaling complexes. Interestingly, our systems-level overview revealed that one signaling intermediate, active Rho, was enriched in the invagination in up to 40% of the cell couples that showed accumulation (fig. S9). We therefore tested the involvement of Rho in turnover of the invagination. We

incubated 5C.C7 T cells with the Rho inhibitor exoenzyme C3 transferase covalently linked to a cell-penetrating moiety through a disulfide bond (Cytoskeleton Inc.) and activated the T cells with CH27 B cell lymphoma APCs transfected with the CD2 ligand CD48GFP (as a marker for receptor enrichment in the invagination) in the presence of 10 μM MCC antigenic peptide. Consistent with an established role for RhoA in T cell-APC coupling (*3*, *4*), only 40.5% of T cells proceeded to form a tight cell couple after initial APC contact in the presence of the Rho inhibitor in comparison to 63% of T cells in its absence ($p < 0.001$). Resolution of the T cell invagination was delayed in the presence of C3 transferase, as invagination-enriched CD48-CD2 couples occurred significantly ($p \leq 0.05$) more frequently at all time points ≥ 100 s after formation of a tight cell couple (fig. S10). Thus, Rho is a critical regulator of the resolution of the large T cell invagination. Our systems-level description of spatiotemporal patterning in T cell activation thus was critical in establishing that invagination-enriched receptors were relatively poor in associated signaling intermediates, and in the identification of a new role for Rho by revealing its surprising accumulation in the large T cell invagination.

Methods

Image acquisition and analysis

T cell-APC interactions in the presence of 10% fetal bovine serum were imaged at 37°C with a 40 x/NA = 1.3 oil objective. Every 20 seconds, 1 DIC and 21 fluorescence images were acquired. The 21 fluorescence images spanned 20 μm in the z-plane at 1 μm intervals. A piezoelectric z-motor was used for rapid adjustments along the z-plane. A MicroMax cooled CCD camera (Princeton Instruments) with a 1300 x 1030 chip size and a pixel size of 6.7 x 6.7 μm was used at 2 x 2 binning with an acquisition time of 200 ms to acquire the images. All 21 images of one z stack were streamed into computer memory for the fastest camera readout. Thus, a single z stack was acquired in 7 s.

Cell coupling was determined in the DIC images only, without regard for the fluorescence information. The formation of a tight cell couple, time 0 in our analysis, was defined as either the first time point with a fully spread T cell-APC interface or 40 s after first membrane contact, whichever occurred first. This definition of tight cell coupling is a compromise between synchronization of data in time versus space. More than 90% of the cell couples formed a fully spread interface upon first contact or 20 s thereafter. However, the remainder of the cell couples persisted with a small initial contact area up to 2 min before forming a wide interface. Exclusive definition of tight cell coupling by interface spreading (that is, synchronization in space based on the argument that only a wide interface enables full receptor-ligand engagement), would allow longer initial small contacts in the non-prototypical subset (< 10%) of the cell couples. Comparison of the accumulation dynamics of the TCRζ-GFP and TCRε-GFP fusion proteins (fig. S6) illustrates that the chosen synchronization displayed a variability of less than 20 s.

Patterns of accumulation of sensors at the interface were determined with the Metamorph software package. Fluorescence data were analyzed at 12 time points, from -40 s to 2 min in 20 sec intervals, and then at 3 min, 5 min, and 7 min. Data used for this analysis were a maximum projection for the identification of the x and y coordinates of an area of accumulation and maximum-type three-dimensional reconstructions or the raw 3D stacks for the determination of the z coordinates. Fluorescence intensities were displayed as a rainbow false-color scale for an initial intensity overview such that the entire range of cellular fluorescence was covered by the full rainbow color scale. Through the use of the known quantitative differences in fluorescence intensity underlying the color scale, a region of accumulation of a given sensor was defined as a region with an average fluorescence intensity of > 135% of the background cellular fluorescence, as verified by explicit intensity measurements. A time point was scored as “no accumulation” if the fluorescence intensity within a distinct area of interface accumulation was < 135% of the background intensity of cellular fluorescence. Areas of interface accumulation that were contiguous with those of noninterface accumulation were scored as no accumulation, as it was uncertain whether such accumulation was dependent on receptor engagement at the T cell-APC interface or reflected rare, uneven distributions of fluorescence. To classify the spatial features of a bona fide area of accumulation, five mutually exclusive interface patterns were used: central, invagination, diffuse, lamellal, and peripheral, as defined by strict geometrical constraints (listed in Fig. 2). Geometrical parameters were measured with the region measurement function of the Metamorph software package. When an area

of accumulation fulfilled the criteria for two patterns, for example, accumulation at 140% above background cellular fluorescence over all of the interface (diffuse) and at 180% above the background cellular fluorescence at the center of the interface (central), the smaller pattern (central in this example) was scored. Distal accumulation was scored independently of the interface patterns; that is, a T cell could display one of the five interface patterns together with that of distal accumulation. Distal accumulation was consequently not included in the "any accumulation" category. To ensure the reliability of this analysis, data were routinely analyzed by two investigators independently. Data for each experimental condition were displayed as the percentage of cell couples that showed accumulation in any of the six patterns at each time point. Standard errors were calculated. Comparison of the independent pattern analyses of the TCRζ-GFP and TCRε-GFP fusion proteins (fig. S6) illustrates the reliability of this analysis. For the graphical display in Fig. 3, accumulation of a given sensor in any pattern in > 30% of the cell couples at each time point was denoted by a light shade of that sensor's color (in the caption and in the figure), whereas accumulation in > 60% of cell couples was denoted in a darker shade of the same color. Where accumulation occurred in < 30% of the cell couples, sensors were not listed. When a specific pattern occurred in > 50% of the T cells with accumulation, only this pattern was depicted; otherwise the two or three most dominant patterns were given. All sensors, with the exception of SAP-GFP, showed accumulation for at least one time point. Tubulin-GFP and the Arf6 sensor showed only intracellular punctuate patterning that is not captured by our pattern classification (fig. S16). Nuclear translocation of NFAT-GFP is displayed separately (fig. S4).

The spatial preference index used in Fig. 5, fig. S12, and fig. S14 was calculated by the following formula:

$$\text{Spatial preference index} = \log\left[\frac{\%\text{ cell couples with central accumulation} + \%\text{ cell couples with diffuse accumulation}}{\%\text{ cell couples with peripheral accumulation} + \%\text{ cell couples with diffuse accumulation}}\right] \times \%\text{ cell couples with any accumulation}$$

A value of 1 or –1 indicates almost exclusive central or peripheral accumulation, respectively, whereas a value of 0 indicates a balance between central and peripheral accumulation. For the determination of nuclear translocation of NFAT-GFP, line scans through the center of the T cell were used to determine whether NFAT-GFP fluorescence was more intense in the cytoplasm or the nucleus. T cells were scored as 0 for a cytoplasmic accumulation of NFAT-GFP, 0.5 for an even distribution between the cytoplasm and the nucleus, and 1 for a nuclear distribution.

For spinning disk confocal microscopy, 41 z planes spaced 0.4 μm apart were acquired every 30 s on a Perkin Elmer Ultraview ERS microscope with a 63 x oil objective. A Hamamatsu Orca AG camera was used with a 400 ms acquisition time and 2 x 2 binning; thus, a single z stack was acquired in 25 s. Data were analyzed with Imaris Software (Bitplane). The area of accumulation and the entire cell were identified in the three-dimensional fluorescence image stacks by the software's segmentation tool and region properties were measured. To ensure reliability of this analysis, data were routinely analyzed by two investigators independently.

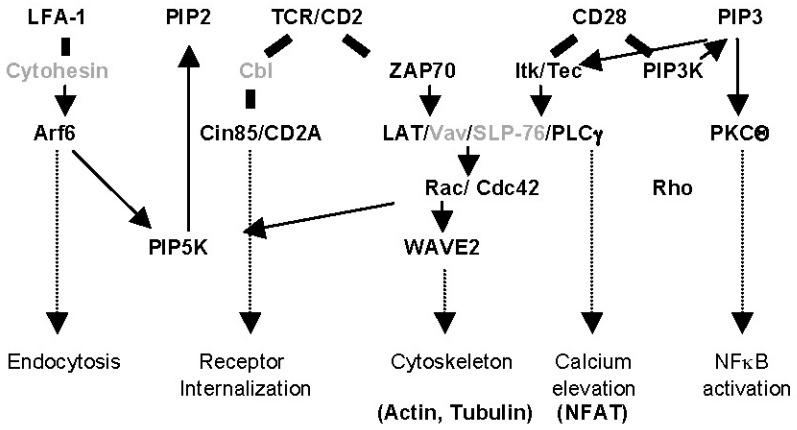

Fig. S1. Components of T cell activation examined in this study. Key T cell signaling intermediates studied (in black) and selected molecular interactions thereof are shown. Thick lines indicate direct molecular interactions, whereas arrows indicate the activation or generation of targets in molecular interactions.

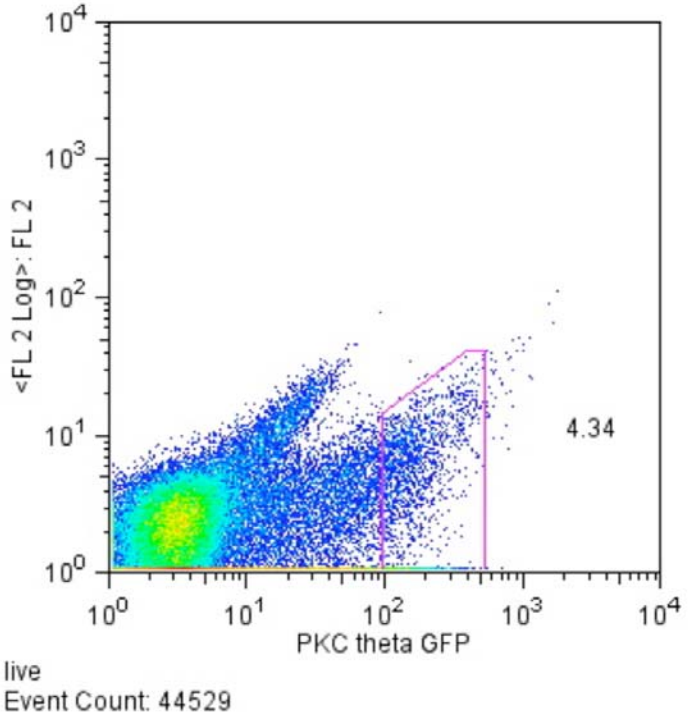

Fig. S2. FACS-based sorting of sensor-expressing T cells. A representative flow cytometry plot of PKCθ-GFP-transduced 5C.C7 T cells is shown. T cells were gated on live cells on the basis of forward and side scatter. GFP fluorescence intensity is displayed on the x-axis, cellular autofluorescence is displayed in the phycoerythrin channel (FL2) on the y-axis. Dead cells were secondarily eliminated as cells displaying increased fluorescence intensity in both channels. The sort gate is indicated in the pink box with the percentage of live cells therein. The same gating was used for all other sensors.

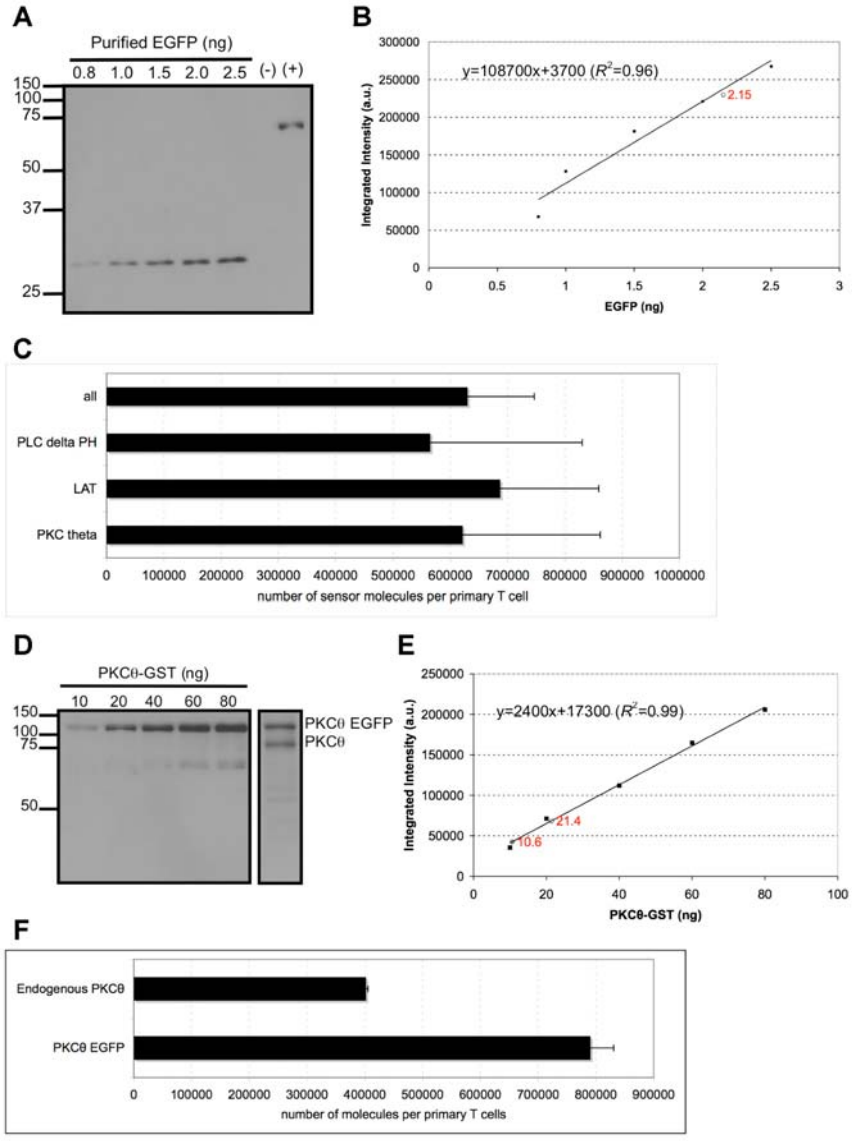

Fig. S3. Quantification of the abundance of biosensors and endogenous PKCθ. (**A**) Two cell extracts were generated. The first, from 40,000 primary T cells that had been retrovirally transduced to express LAT-GFP and that had been sorted by FACS for a 5-fold range of low abundance of GFP (+) and the second, from 40,000 nontransduced, live, sorted primary T cells (-). Western blotting analysis for GFP is shown with both cell extracts loaded next to a series of increasing amounts of purified EGFP, as indicated. (**B**) Integrated band intensities are plotted against the amounts of purified EGFP. The data point from the cell extract from the LAT-GFP-transduced primary T cell is given as an open circle with the calculated amount of GFP in red (in ng). One quantification experiment representative of 4 is shown. (**C**) The numbers of molecules per primary T cell of fusion proteins of GFP fused to PKCθ, LAT, and the PH domain of PLC-δ in transduced and FACS-sorted primary T cells were determined as described above. A summary of all data is shown. Three to four quantifications were performed for each construct. The corresponding molar concentrations are 4.8 ± 0.9 μM for all sensors combined, and 4.7, 5.2, and 4.3 μM for the PKCθ, LAT, and PLCδ-PH GFP fusion proteins, respectively. (**D**) A cell extract generated from 200,000 primary T cells that had been transduced to express PKCθ-GFP and were sorted for a 5-fold range of low GFP abundance was loaded next to a series of increasing amounts of purified PKCθ-GST, as indicated. The bands for GFP-tagged and endogenous PKCθ are marked. Both parts of the panel are derived from the same blot; with only intermittent unrelated lanes were removed. (**E**) Integrated band intensities were measured and plotted against the amounts of PKCθ-GST. One quantification experiment representative of 3 is shown. (**F**) The summary of all experimental repetitions from panels D and E is given. The corresponding molar concentrations for PKCθ-GFP and endogenous PKCθ were 6.0 and 3.0 μM, respectively.

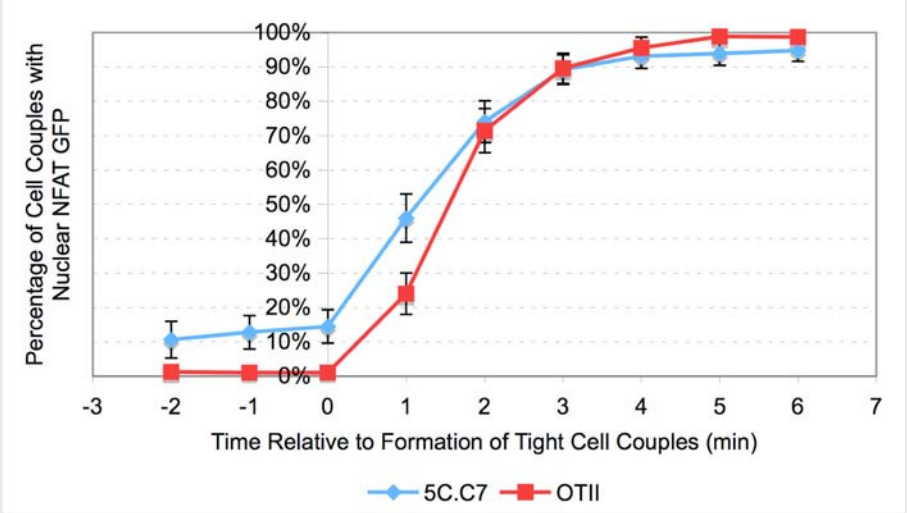

Fig. S4. Rapid nuclear translocation of NFAT. The percentage of cell couples that contained NFAT-GFP in the nucleus are given with standard errors for the interaction of either NFAT-GFP-transduced primary 5C.C7 T cells with CH27 APCs in the presence of 10 mM MCC antigenic peptide or NFAT-GFP-transduced primary OTII T cells with IFN-γ-induced DC2.4 APCs in the presence of 10 μM Ova peptide relative to the total number of tight cell couples formed. Differences at time points 0 and 1 min were significant ($p < 0.05$). 52 cell couples were analyzed for 5C.C7 T cells, whereas 50 cell couples were analyzed in the case of OTII T cells.

CH27 B cell lymphoma

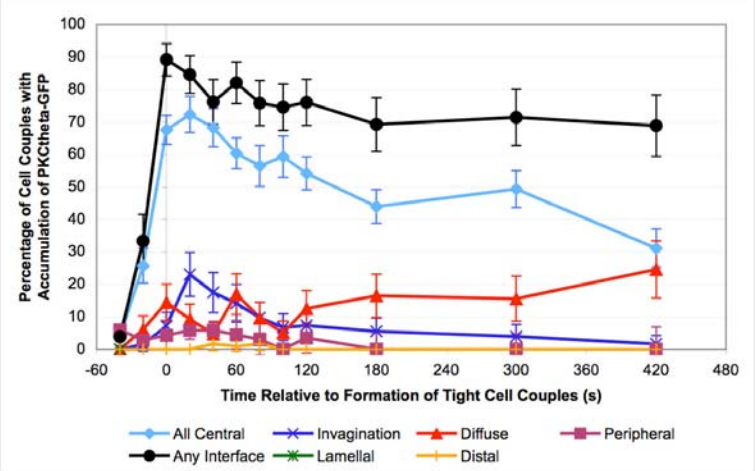

Bone marrow-derived dendritic cell

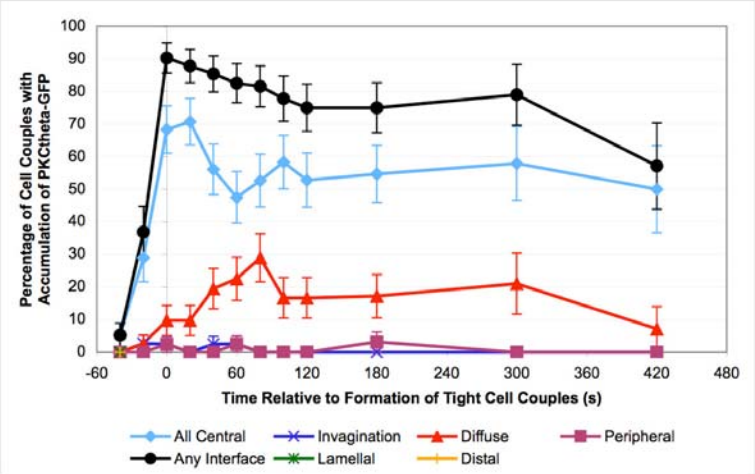

Fig. S5. Patterning of PKCθ in activated 5C.C7 T cells. Stimulation of primed 5C.C7 T cells by B cell lymphoma APCs or primary dendritic cells triggers comparable patterning of PKCθ. Primed, primary 5C.C7 T cells were transduced with PKCθ-GFP and stimulated with CH27 B cell lymphoma APCs (top) or bone marrow-derived dendritic cells (bottom) in the presence of 10 μM MCC antigenic peptide. Spatiotemporal patterns of PKCθ–GFP are displayed similar to those in Fig. 1C. For CH27-stimulated T cells, 111 cell couples were analyzed, whereas in experiments involving dendritic cells, 41 cell couples were analyzed.

Receptors

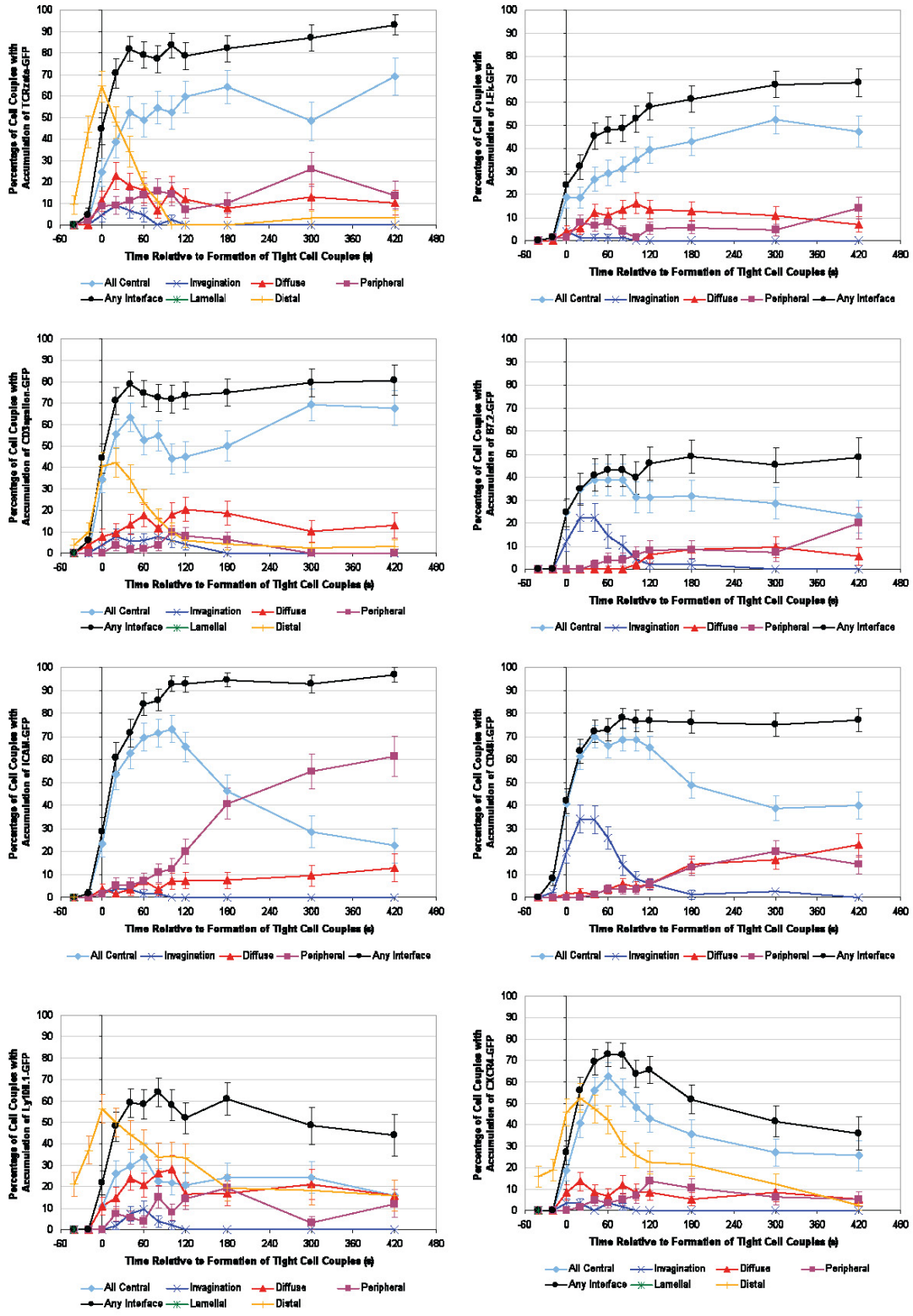

Fig. S6

Proximal Signaling

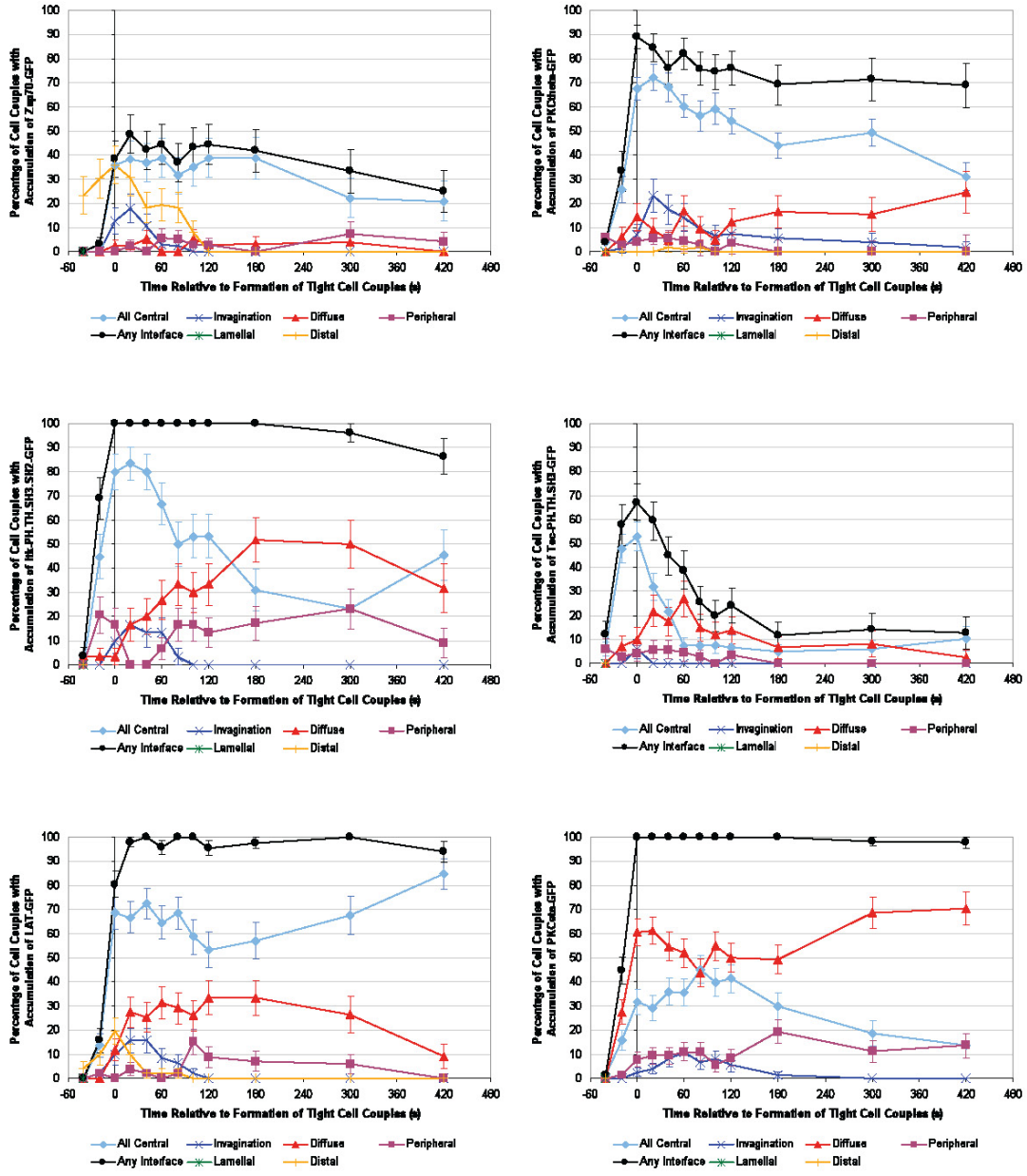

Fig. S6 continued

Lipids

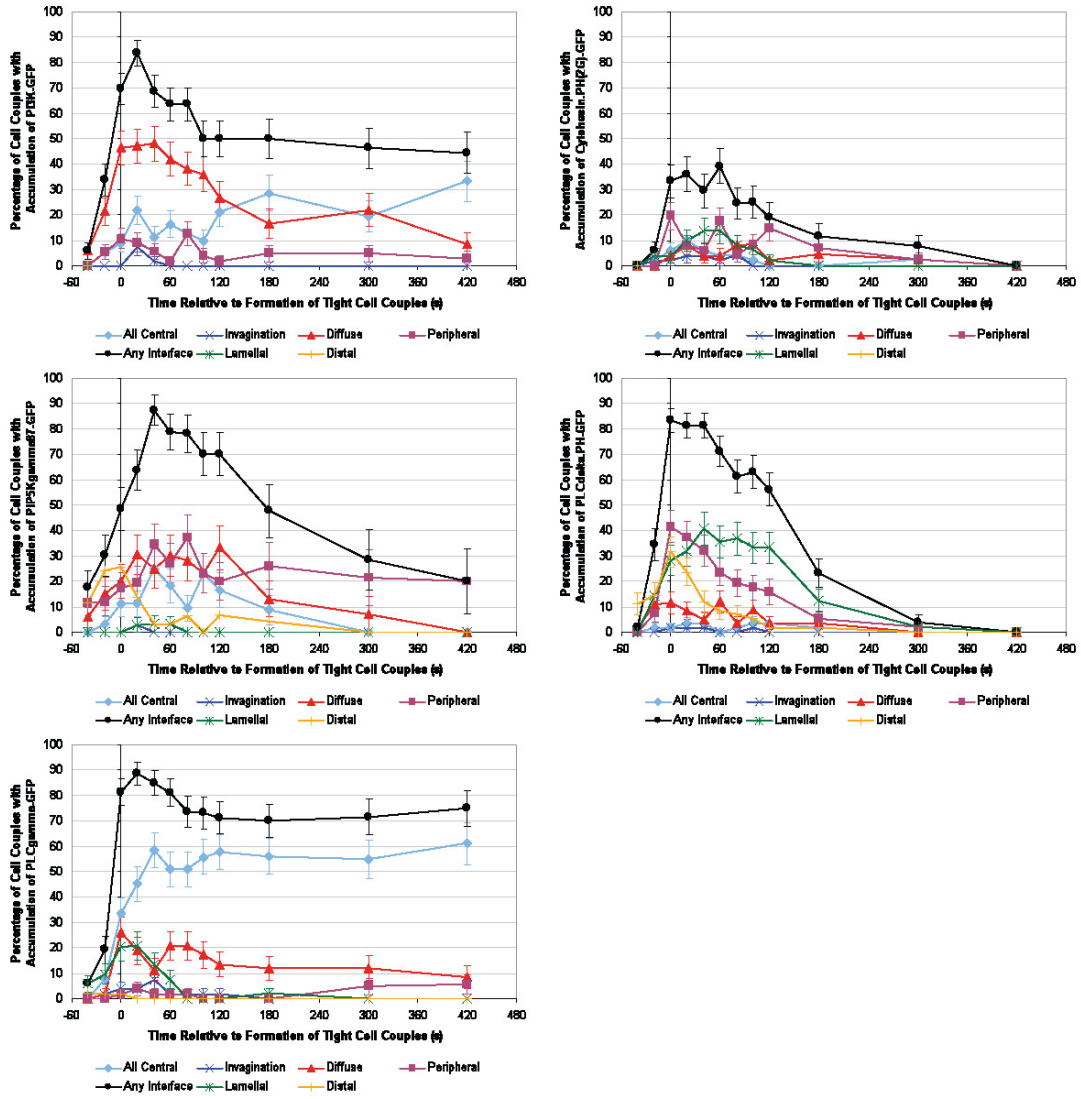

Endocytic Adaptors

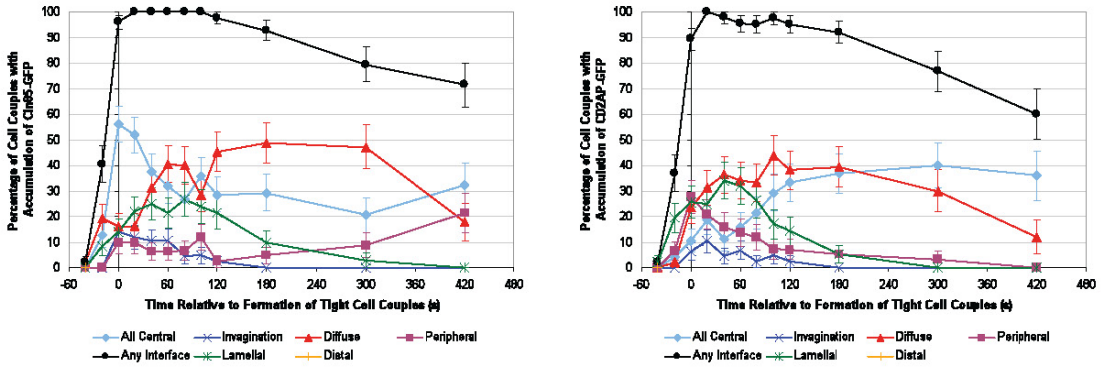

Fig. S6 continued

Rho GTPases

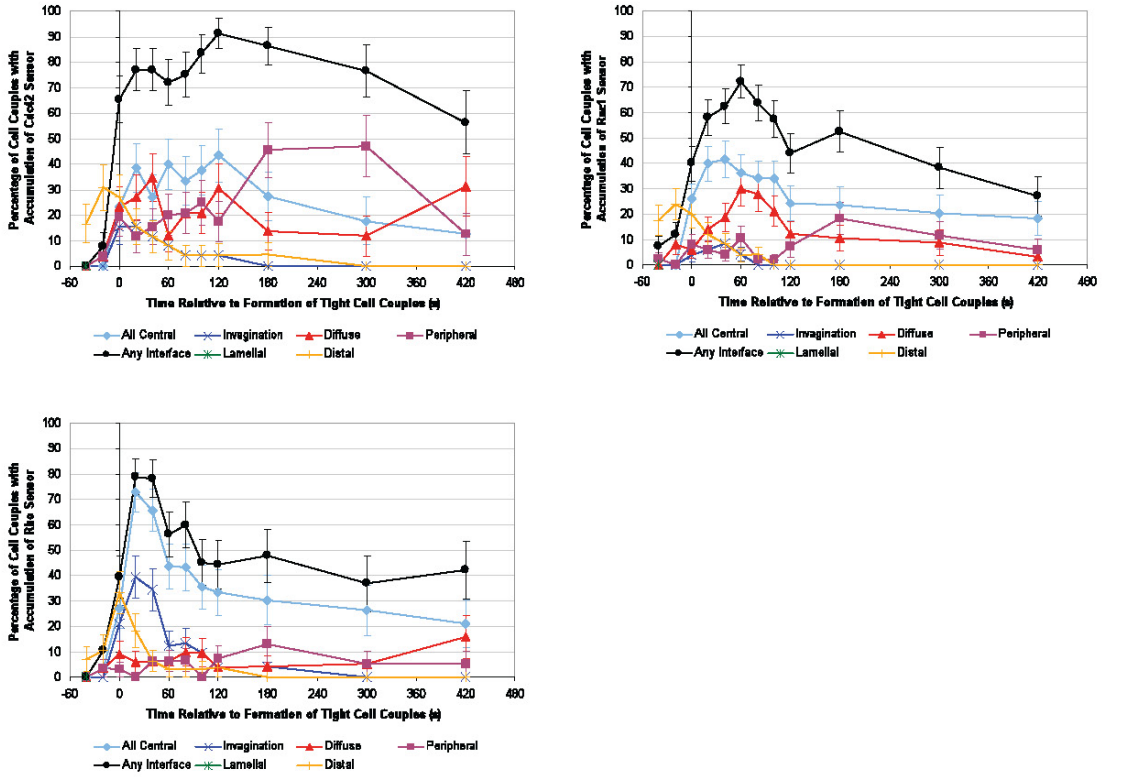

Cytoskeleton

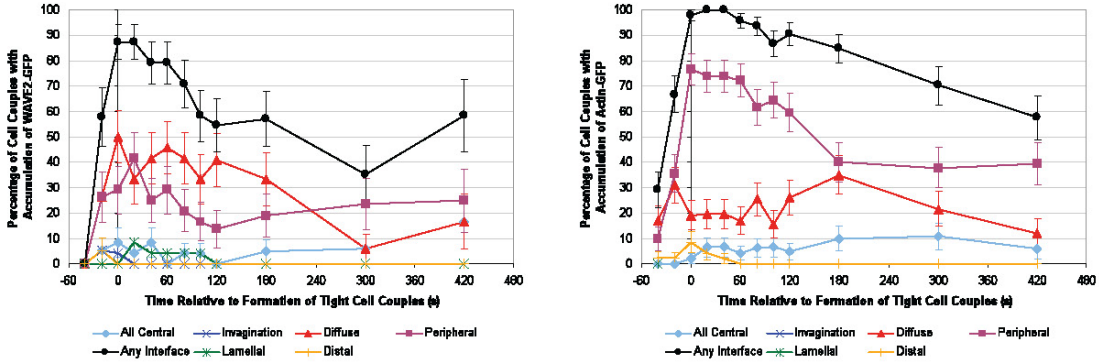

Fig. S6. Highly diverse spatiotemporal patterning during T cell activation. In the interaction of primary 5C.C7 T cells with CH27 APCs in the presence of 10 μM MCC antigenic peptide, the percentage occurrence of each of the six patterns of sensor accumulation (see Fig. 2) was determined at 12 time points as indicated for 30 molecules involved in T cell activation (see Table 1 for list). For the 26 sensors that could be analyzed with the pattern analysis, the graphs display the percentage of cell couples with accumulation in the indicated patterns (with standard errors) relative to the number of tight cell couples formed. All sensors with the exception of SAP-GFP showed accumulation during at least one time point. Tubulin-GFP and the Arf6 sensor showed only intracellular punctuate patterning that is not captured by our pattern classification (fig. S16). Nuclear translocation of NFAT-GFP is displayed separately (fig. S4). Between 24 and 111 cell couples (53 on average) were analyzed per sensor (table S2). These data are represented graphically in Fig. 3.

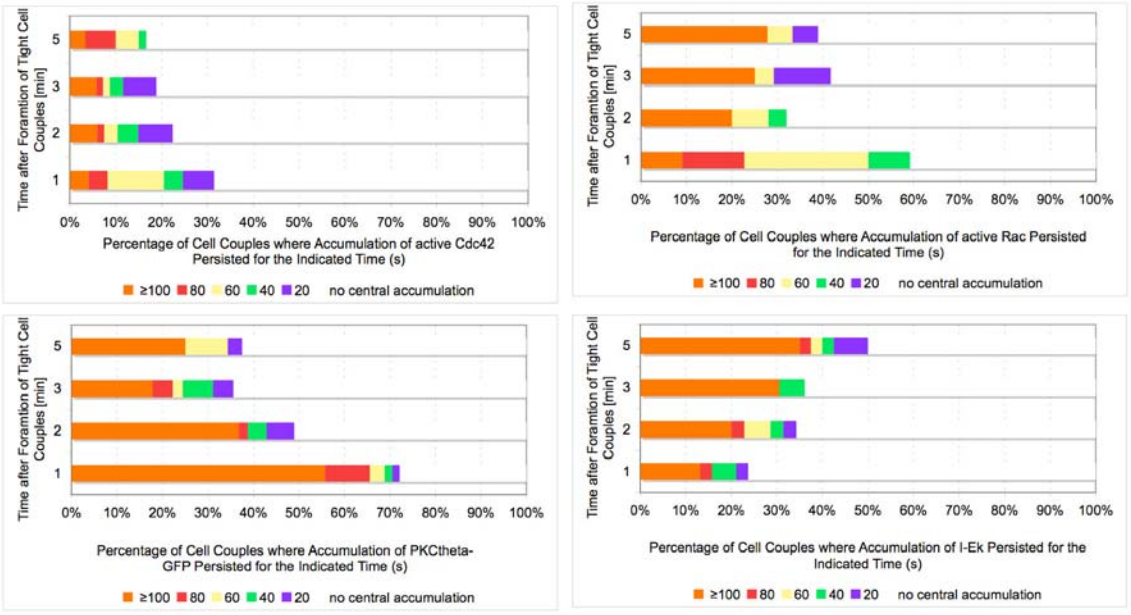

Fig. S7. Dynamic nature of spatiotemporal patterns. Primary 5C.C7 T cells were transduced with the indicated sensors and activated with CH27 APCs in the presence of 10 μM MCC peptide. The graphs display the percentage of cell couples that showed central accumulation of sensors at 1, 3, 5, and 7 min after the formation of a tight cell couple (as indicated on the right of each panel), in which the central accumulation lasted for 20, 40, 60, 80, or ≥ 100 s (as indicated on the bottom of each panel). Between 25 and 73 cell couples (average 44) were analyzed per sensor, and a subset of the data is displayed in Fig. 3 and fig. S6.

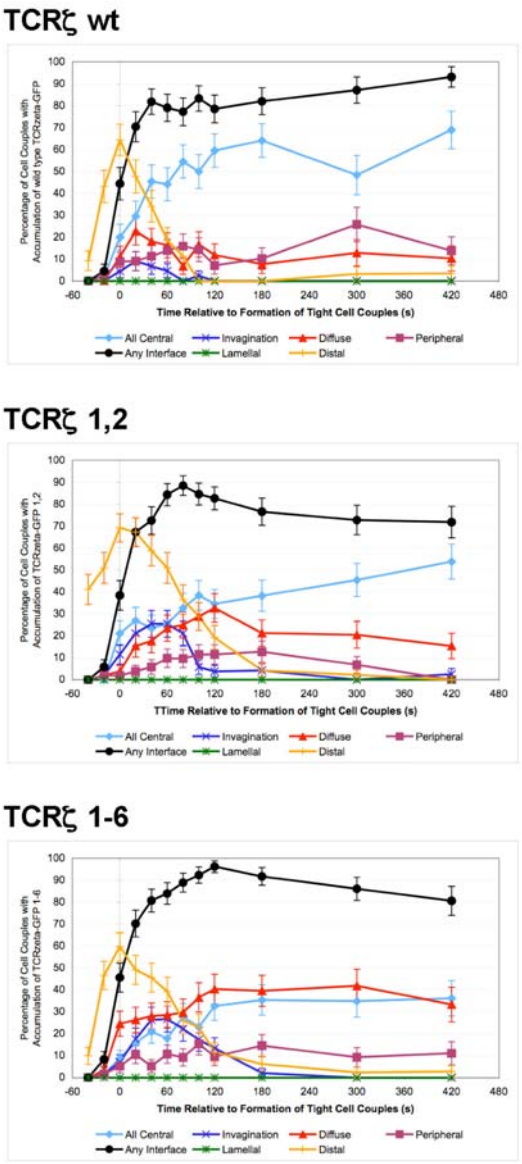

Fig. S8. Requirement for TCRζ ITAMs for effective recruitment of TCR to the cSMAC signaling complex. Primary 5C.C7 TCR transgenic T cells were retrovirally transduced to express WT or mutant TCRζ proteins, as indicated. Transduced cells were activated by CH27 B cell lymphoma APCs in the presence of 10 μM MCC peptide. The percentage of cell couples that showed accumulation in the indicated patterns are given (with standard errors) relative to the number of tight T cell-APC couples formed as a function of time. Between 45 and 60 cell couples were analyzed for each condition (table S2). Differences in the percentage of accumulation of mutant TCRζ proteins in the invagination relative to that of WT TCRζ were significant ($p < 0.01$) at time points of 40 to 80 s for TCRζ 1,2 and 40 to 120 s for TCRζ 1-6. Differences in accumulation in the distal pattern relative to that of WT TCRζ were also significant ($p < 0.05$) at time points of 20 to 180 s for TCRζ 1,2 and 60 to 180 s for TCRζ 1-6. Differences in accumulation in the surface central pattern relative to that of WT TCRζ were significant ($p < 0.05$) at time points 40, 80, and 120 s for TCRζ 1,2 and at 40 to 180 s for TCRζ 1-6.

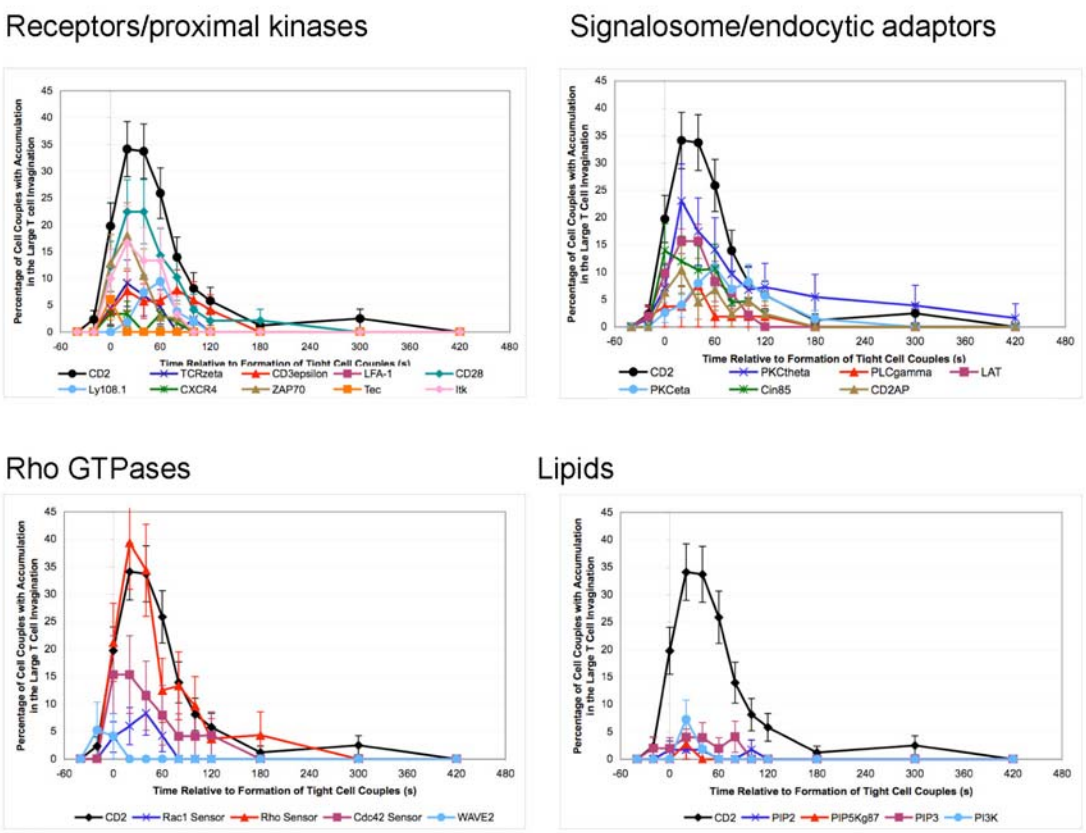

Fig. S9. Enrichment of sensors in the large T cell invagination. Primary 5C.C7 T cells were transduced with the indicated sensors and activated with CH27 APCs in the presence of 10 μM MCC peptide. The percentage of cell couples that showed accumulation of the indicated sensors in the large T cell invagination is given with standard errors. These data are the same as those shown in fig. S6. To illustrate the significance of the data, statistical significance for selected pair-wise sensor combinations is given: Differences relative to CD2 were significant with $p < 0.05$ for PKCθ at time points 0 and 40 s and with $p < 0.001$ when pooled over time points 0 to 100 s. Differences relative to CD2 were significant with $p < 0.05$ for ZAP-70 at time points 40 and 60 s and with $p < 0.001$ when pooled over the time points from 0 to 100. Differences relative to CD2 were significant with $p < 0.05$ for LAT at times 20, 40, and 60 s and with $p < 0.001$ when pooled over the time points from 0 to 100. Differences relative to active Rho were significant with $p < 0.05$ for active Rac at time points 0, 20, 40, and 80 s and with $p < 0.001$ when pooled over the time points from 0 to 100 s. Differences relative to active Rho are significant with $p < 0.005$ for active Cdc42 when pooled over the time points 0 to 100 s.

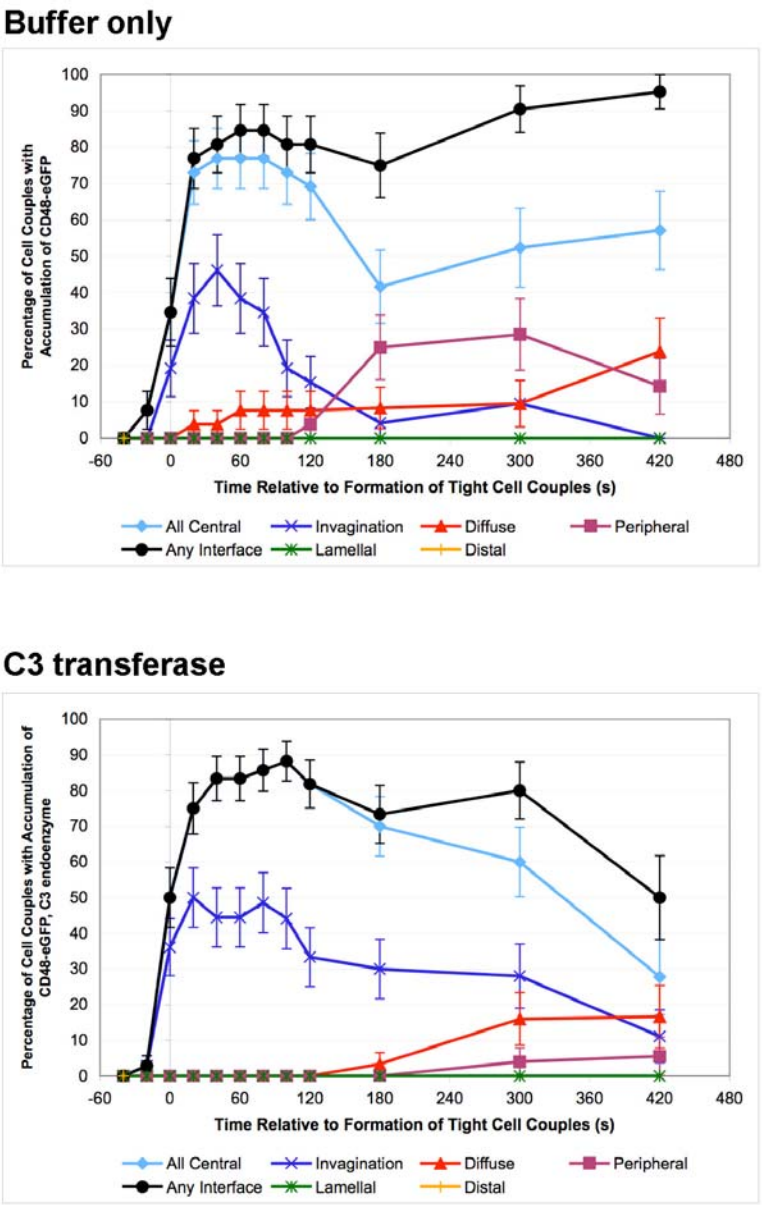

Fig. S10. Requirement for Rho activity for the resolution of the large T cell invagination. The percentage occurrence of each of the six accumulation patterns in primary 5C.C7 T cells that interacted with CD48iGFP-transfected CH27 APCs in the presence of 10 μM MCC anitgenic peptide was determined at 12 time points. T cells were pretreated (for 2 or 4 hours with identical results) with buffer alone (top) or with 1 μg/ml of cell-permeable exoenzyme C3 transferase (bottom). 36 cell couples were analyzed in the treated condition and 26 cell couples were analyzed for cells incubated with buffer alone. The data from those cells treated with buffer alone are part of the CD2 and CD48 data shown in fig. S6. Differences in the occurrence of CD48iGFP accumulation in the invagination pattern were significant with $p \leq 0.05$ at time points of 100 to 420 s.

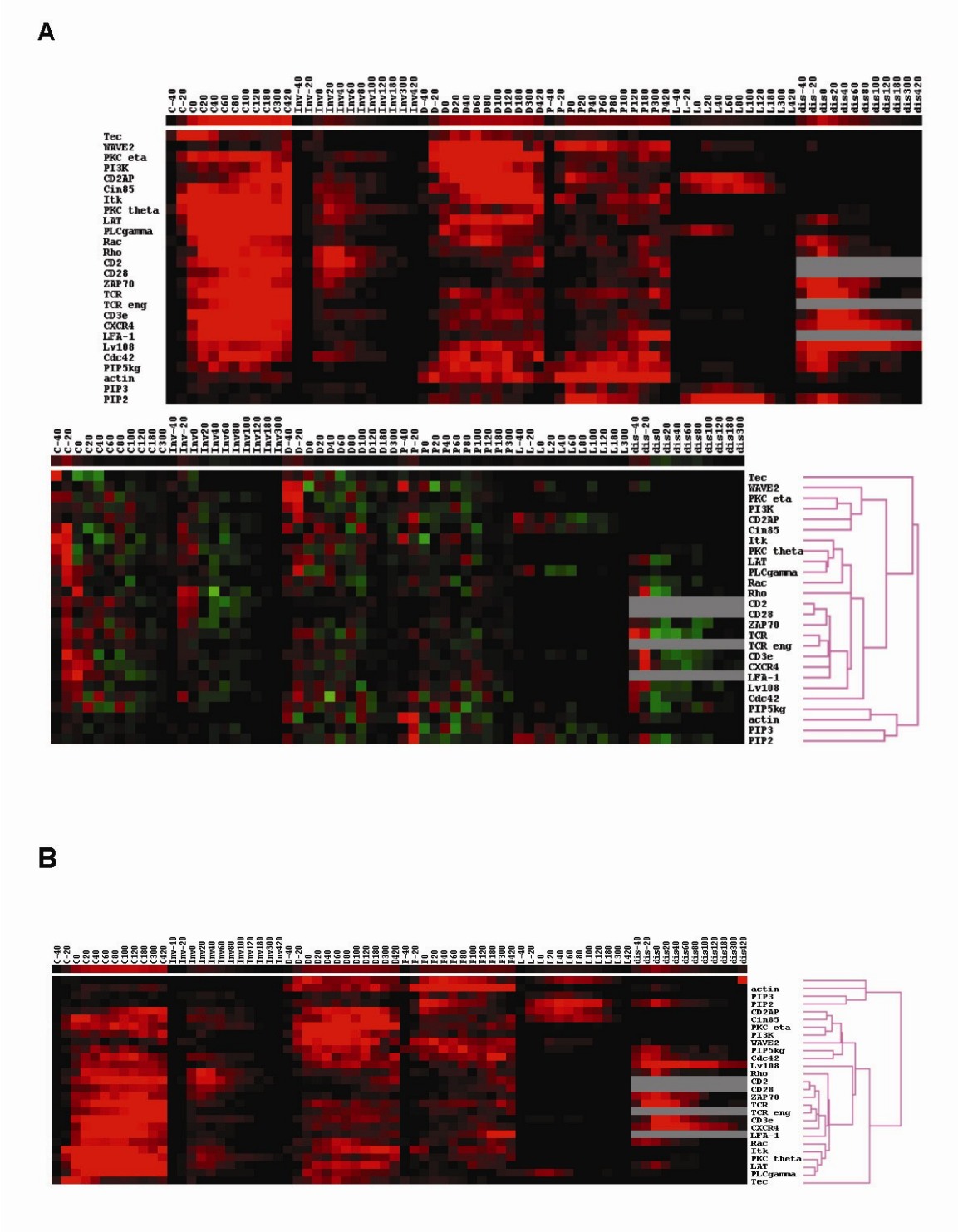

Fig. S11. High diversity of spatiotemporal patterning during T cell activation. A cluster analysis was performed similar to that presented in Fig. 4, but with the inclusion of the distal accumulation pattern (top pane) or removal of the rate of pattern change (bottom panel).

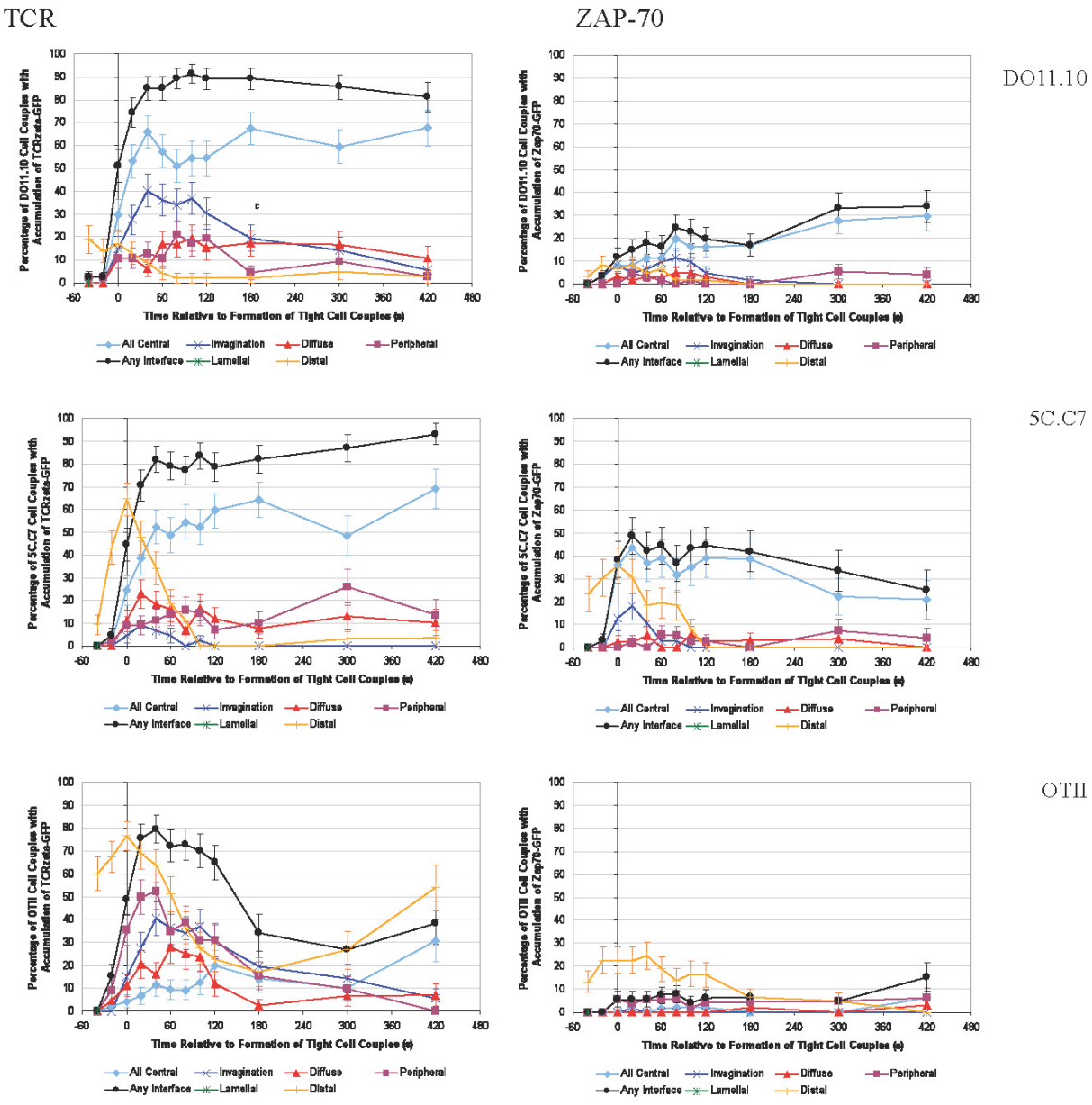
TCR
ZAP-70
DO11.10
5C.C7
OTII
Percentage of DO11.10 Cell Couples with Accumulation of TCRzeta-GFP
Percentage of DO11.10 Cell Couples with Accumulation of Zap70-GFP
Percentage of 5C.C7 Cell Couples with Accumulation of TCRzeta-GFP
Percentage of 5C.C7 Cell Couples with Accumulation of Zap70-GFP
Percentage of OTII Cell Couples with Accumulation of TCRzeta-GFP
Percentage of OTII Cell Couples with Accumulation of Zap70-GFP
Time Relative to Formation of Tight Cell Couples (s)
All Central
Invagination
Diffuse
Peripheral
Any Interface
Lamellal
Distal

Fig. S12

PKCθ

Active Cdc42

DO11.10

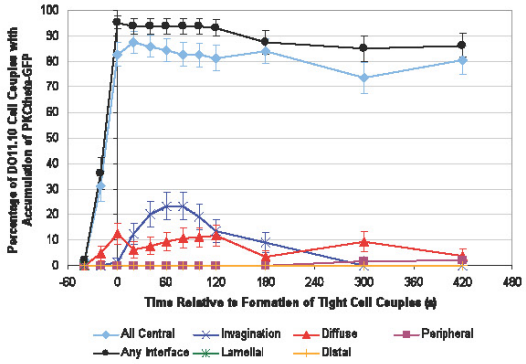

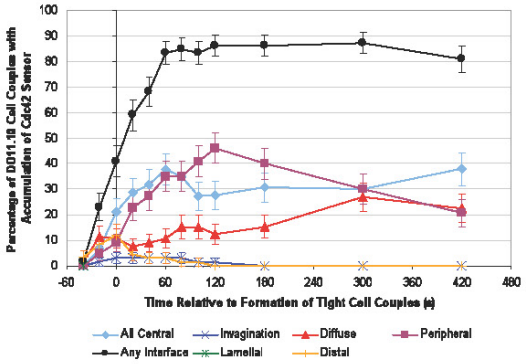

5C.C7

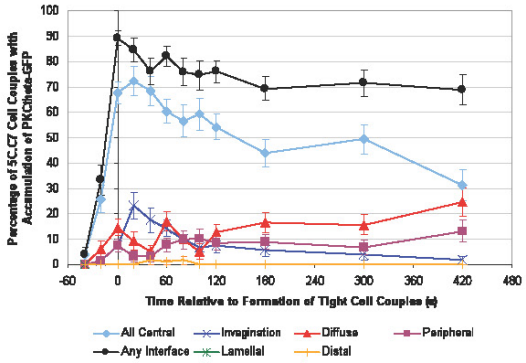

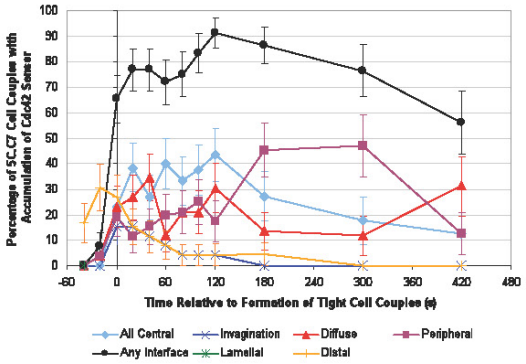

OTII

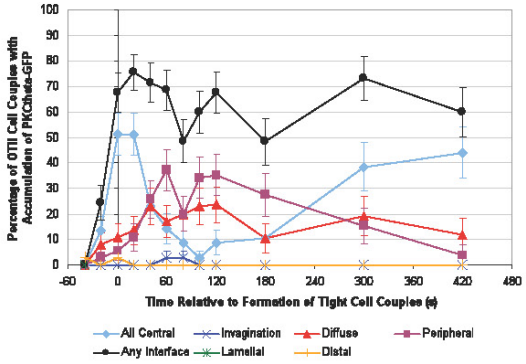

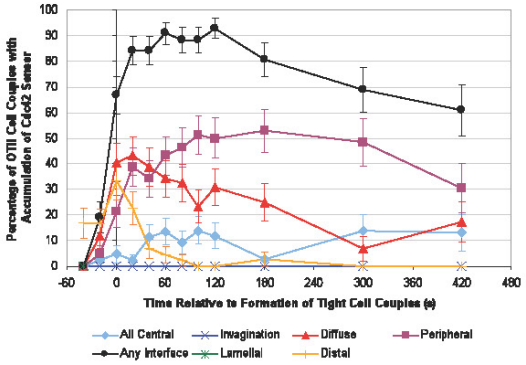

Fig. S12 continued

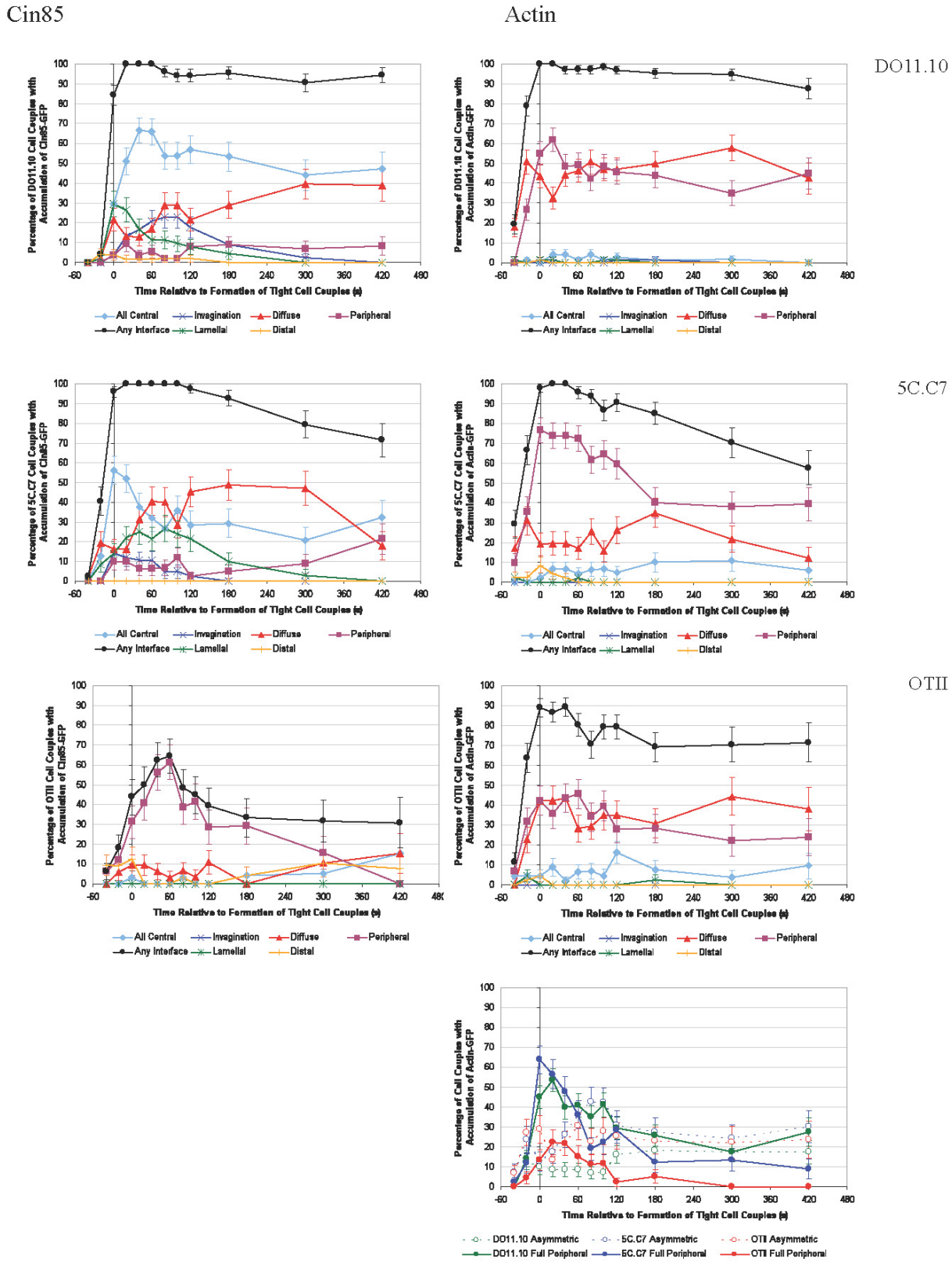

Fig. S12 continued

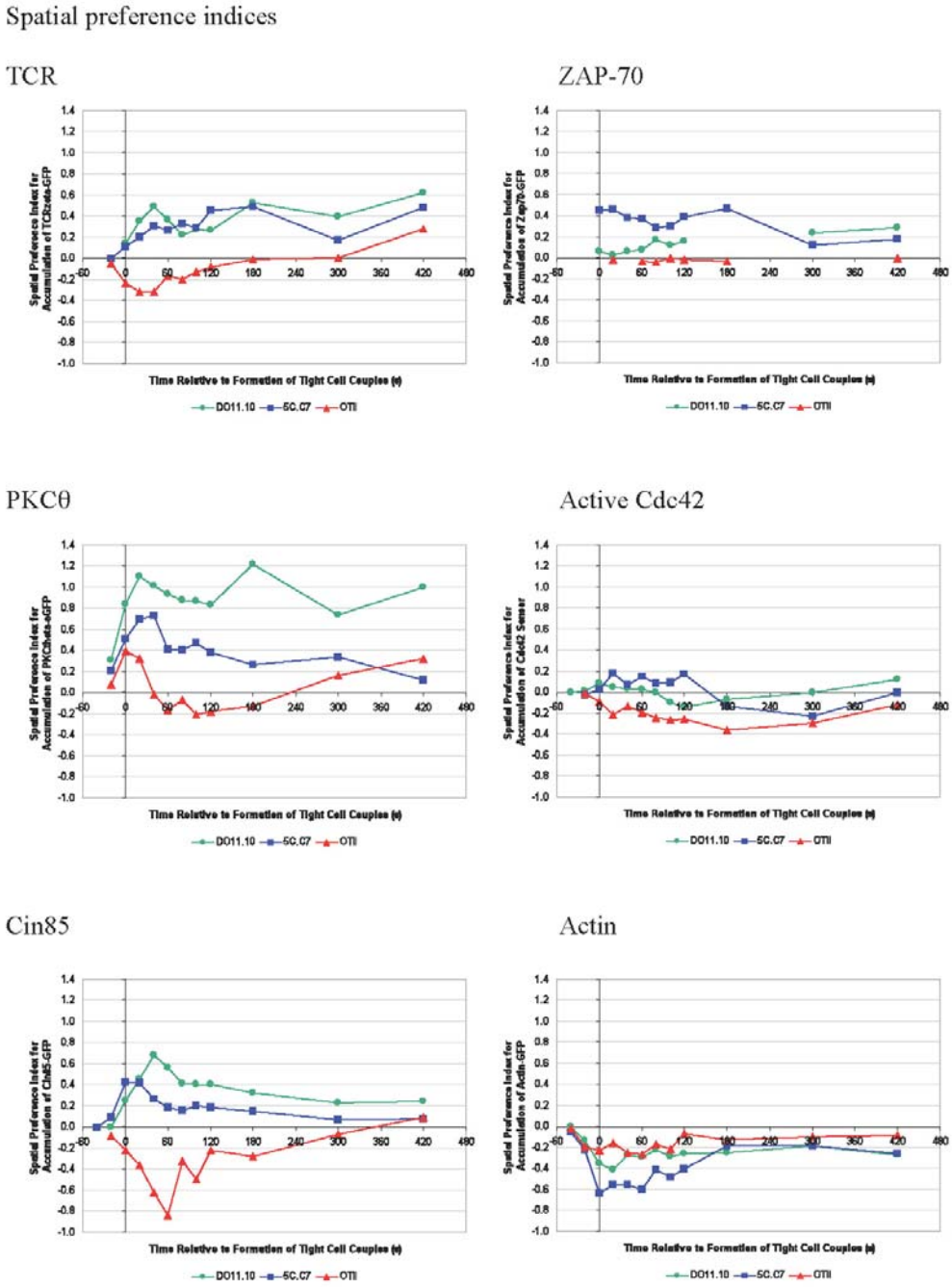

Fig. S12. Variations in spatiotemporal patterning in activated T cells from different TCR transgenic mice. Spatiotemporal patterning of a subset of sensors (as indicated) in the interaction of primary T cells from three different TCR transgenic mice with professional APCs in the presence of 10 mM antigenic peptide is displayed similar to that in fig. S6. OTII T cells were activated with IFN-γ-induced DC2.4 APCs, 5C.C7 T cells with CH27 APCs, and DO11.10 T cells with A20 APCs. Between 27 and 111 cell couples (54 on average) were analyzed for each sensor (table S2). These data are represented graphically in Fig. 5A. The spatial preference index (as defined in the supplementary methods) for all three TCR transgenes together is given at the bottom of each column for easier

comparison, similar to Fig. 5B. At the very bottom of the actin-GFP column, the peripheral pattern is further broken down into two sub-patterns for all three TCR transgenes. If ≤ 25% of the full peripheral circle was covered by the area of accumulation then the peripheral pattern was classified as “asymmetric”. If ≥ 50% of the full peripheral circle was covered by the area of accumulation then the peripheral pattern was classified as “full peripheral”. The asymmetric pattern likely represents the accumulation of actin in individual lamella, with the full peripheral pattern likely representing a stable peripheral adhesion ring. Differences between the percentage of cell couples with full peripheral accumulation between OT II T cells and 5C.C7 T cells were significant with $p < 0.05$ at time points 0 to 60 s, 120, 300, and 420 s. Differences between the percentage of cell couples with full peripheral accumulation between OT II T cells and 5C.C7 T cells were significant with $p < 0.005$ at time points 0, 20, 40, and 120 s. Differences between the percentage of cell couples with full peripheral accumulation between OT II T cells and DO11.10 T cells were significant with $p < 0.05$ at time points -20 s to 60 s, and 420 s. Differences between the percentage of cell couples with full peripheral accumulation between OT II T cells and DO11.10 T cells were significant with $p < 0.005$ at time points 0, 20, and 60 to 420 s.

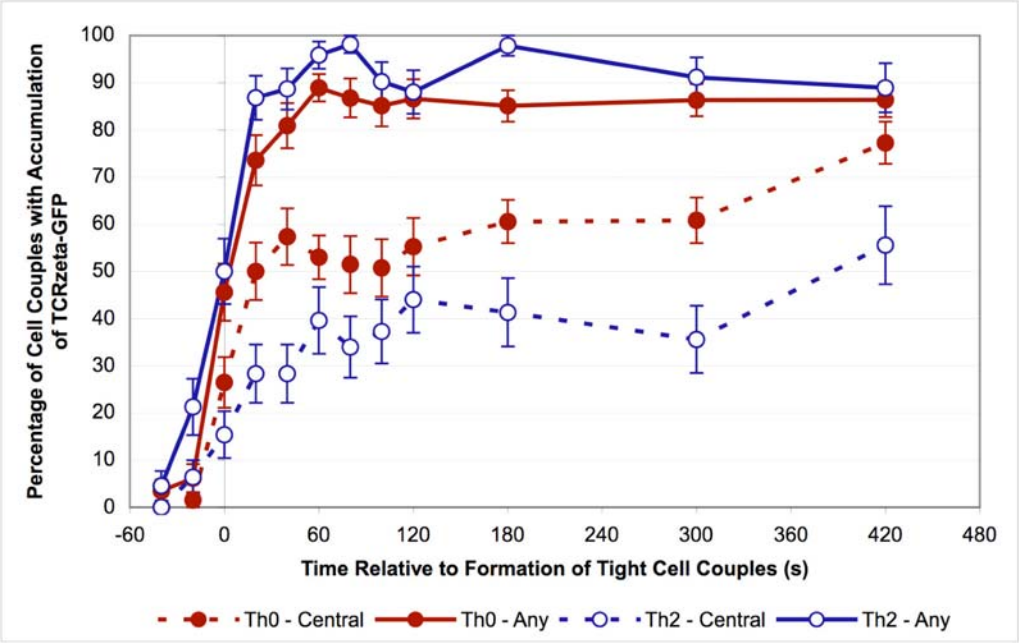

Fig. S13. Reduced TCR clustering in T_H2-polarized DO11.10 T cells. Primary DO11.10 T cells were either differentiated in vitro into T_H2 effector cells (blue) or were left under neutral (T_H0) conditions (red). Cells were then activated by A20 APCs in the presence of 10 μM Ova peptide. The percentage of cell couples with central accumulation (broken line) or any accumulation (solid line) of TCRζ-GFP are presented (with standard errors) relative to the number of tight cell couples formed as a function of time. 53 cell couples were analyzed in the case of T_H2 cells, whereas 68 cell couples were analyzed for T_H0 cells. Differences in the percentage of cell couples with central accumulation were significant ($p < 0.05$) at time points 20, 40, 80, 180, 300, and 420 s. Differences in the percentage of cell couples with central accumulation were significant ($p < 0.01$) at time points 20, 40, 300, and 420 s.

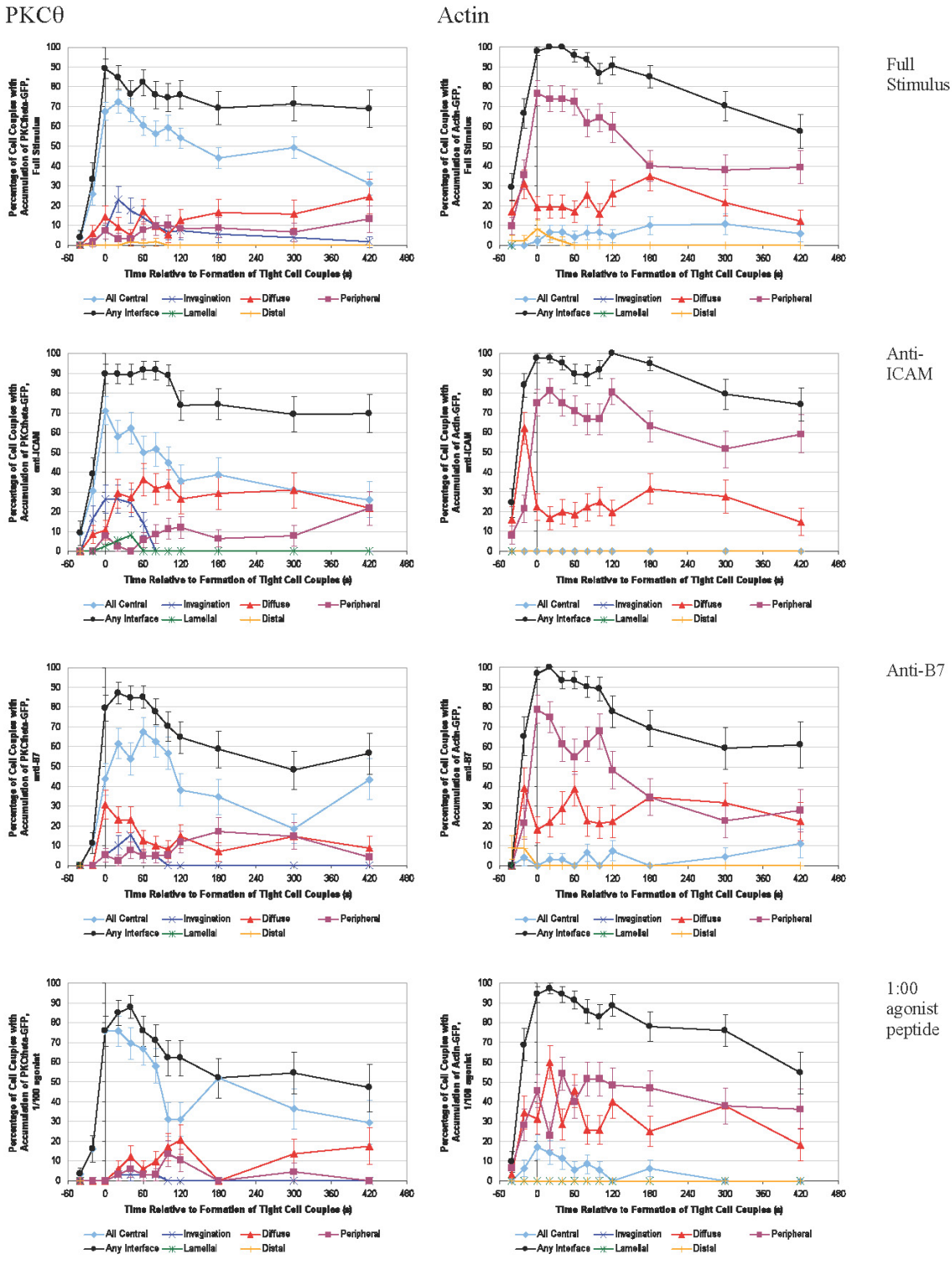
PKCθ
Actin
Full Stimulus
Anti-ICAM
Anti-B7
1:00 agonist peptide
Percentage of Cell Couples with Accumulation of PKCtheta-GFP, Full Stimulus
Percentage of Cell Couples with Accumulation of Actin-GFP, Full Stimulus
Percentage of Cell Couples with Accumulation of PKCtheta-GFP, anti-ICAM
Percentage of Cell Couples with Accumulation of Actin-GFP, anti-ICAM
Percentage of Cell Couples with Accumulation of PKCtheta-GFP, anti-B7
Percentage of Cell Couples with Accumulation of Actin-GFP, anti-B7
Percentage of Cell Couples with Accumulation of PKCtheta-GFP, 1/100 agonist
Percentage of Cell Couples with Accumulation of Actin-GFP, 1/100 agonist
Time Relative to Formation of Tight Cell Couples (s)
All Central
Invagination
Diffuse
Peripheral
Any Interface
Lamellal
Distal

Fig. S14

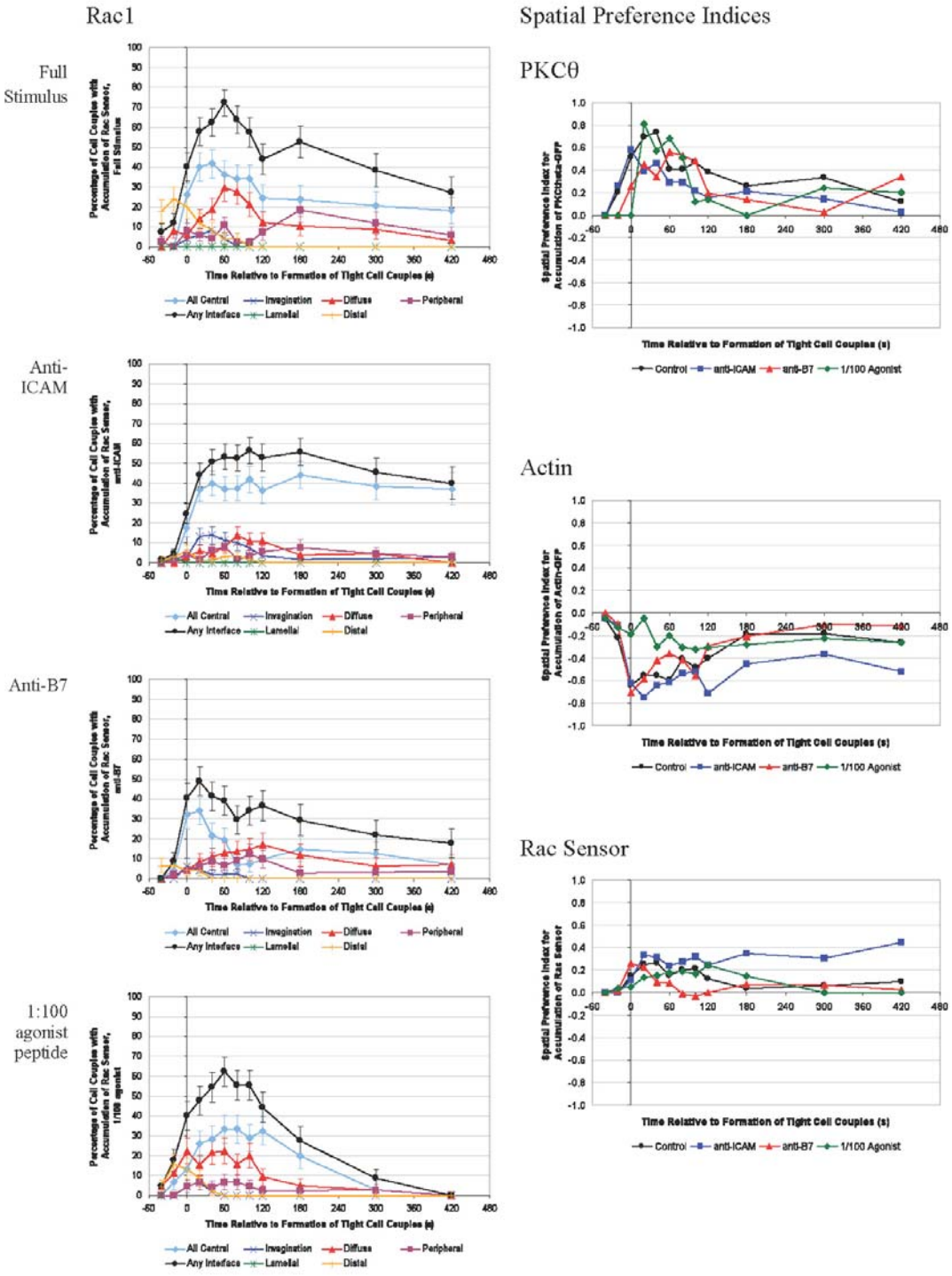

Fig. S14. Regulation of spatiotemporal patterning by costimulation. Spatiotemporal patterning of a subset of the indicated sensors in the interaction of primary 5C.C7 T cells with professional CH27 APCs under varying conditions of T cell activation (as noted) is displayed similarly to that in fig. S6. These data together with published data on ligand-engaged TCR and active Cdc42 *(5, 6)* are represented graphically in Fig. 5E. At the bottom of each column the data above are summarized using the spatial preference index. Between 33 and 69 cell couples (43 on average) were analyzed for each condition (table S2).

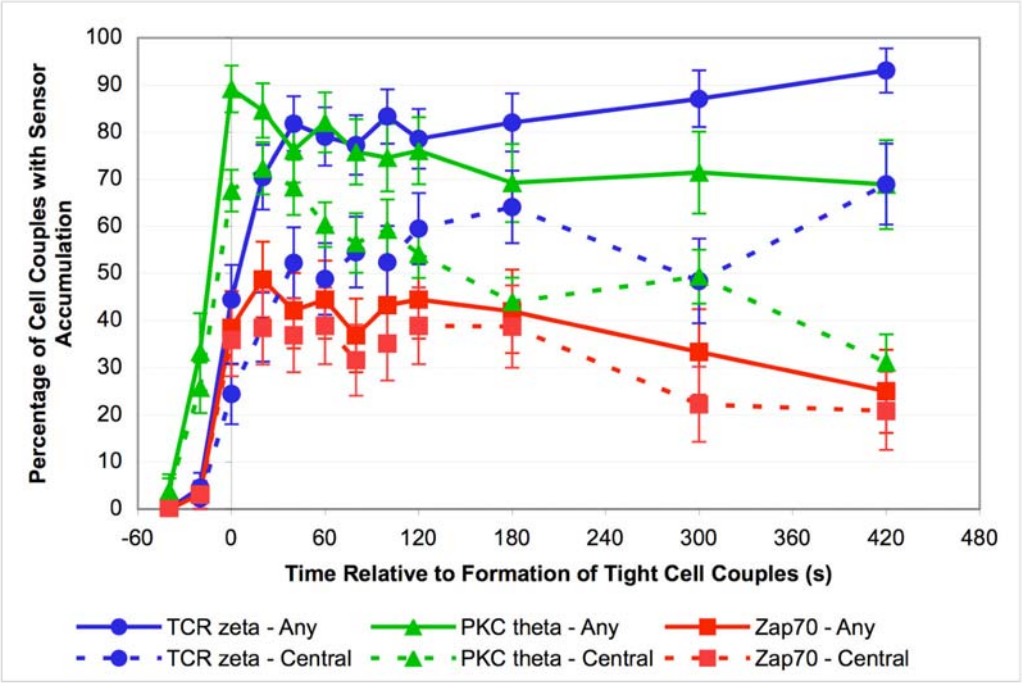

Fig. S15. Delayed central accumulation of the TCR compared to that of its dependent signaling intermediates. Primary 5C.C7 T cells were transduced with the indicated sensors and activated with CH27 APCs in the presence of 10 μM MCC peptide. The percentage of cell couples with accumulation in a central pattern (broken lines) or in any particular pattern (solid lines) is given with standard errors. These data are the same as those shown in fig. S6. Differences relative to TCRζ were significant with $p \leq 0.001$ for PKCθ at time points -20, 0, 20, and 420 s. Differences relative to TCRζ were significant with $p \leq 0.001$ for ZAP-70 at 420 s.

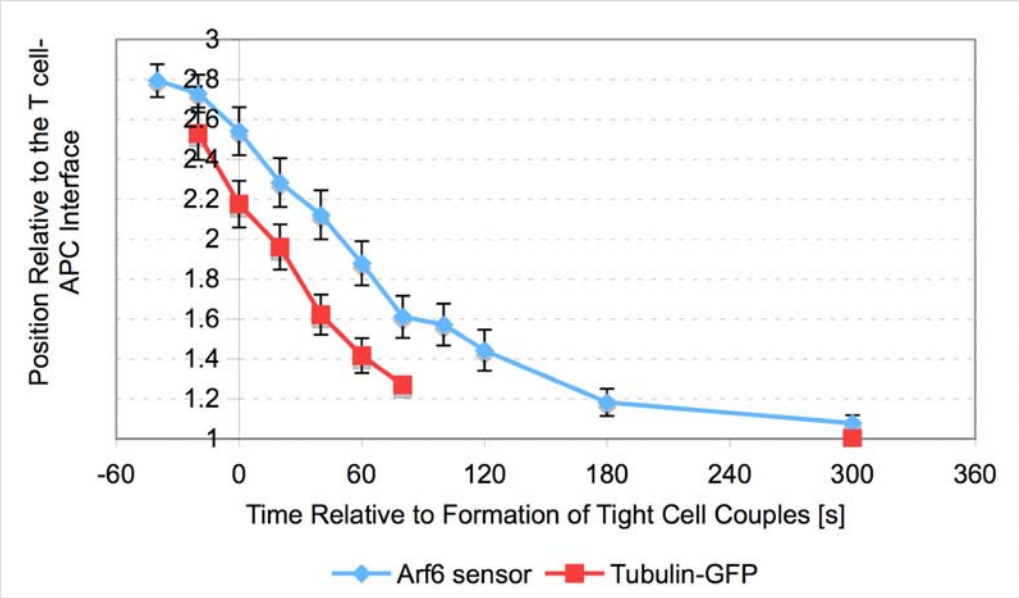

Fig. S16. Similar dynamics of translocation of tubulin-GFP and the Arf6 sensor from the uropod to the interface upon formation of the T cell-APC interface. The average position of the peak fluorescence intensity of tubulin-GFP and the Arf6 sensor is plotted with its standard error against time as previously published (*7*). A position of 1 is closest to the interface, whereas a position of 3 is furthest from the interface. The tubulin-GFP data have been published previously and are shown here for comparative purposes (*7*). Representative images are in (*7*) and movie S25. 53 cell couples were analyzed for the translocation of tubulin-GFP, whereas 37 cell couples were analyzed for the translocation of the Arf6 sensor.

Table S1. List of supplementary movies and a key that includes the sensor monitored, the time of cell coupling, and a description of the critical features observed. Interactions of sensor-transduced 5C.C7 T cells with CH27 B cell lymphoma APCs in the presence of 10 μM MCC agonist peptide are shown in the movies listed. Within in each movie file, the top panel shows differential interference contrast images while the bottom panel shows matching, top-down projections of 3-dimensional sensor fluorescence data displayed in a false color scale (increasing from blue to green, yellow, red, and white). The T cells are identifiable as the smaller cells in the fields of view. Frame separation in each movie is 20 s.

Movie	Sensor	Cell coupling	Critical features (frame numbers)
S1	LAT-GFP	14	Stable central pattern
		44	Late onset
S2	PKCθ-GFP	17	Invagination (17 – 20) and diminishing central pattern
S3	TCRζ-GFP	9	Distal (9 – 11) and late central pattern
S4	TCRζ-GFP	7	Mostly central pattern
S5	TCRζ 1-6-GFP	7	Accumulation in vesicles and central pattern
S6	CD3ε-GFP	5	Stable central pattern
		23	Distal and stable central pattern
S7	ICAM-1-GFP	3	Central to peripheral (e.g. 25) patterning
S8	Ly108-1-GFP	17	Multiple patterns
S9	Ly108-1-GFP	5	Stable central accumulation
S10	CXCR4-GFP	5	Distal (2 – 10) to transient central pattern
		17	Transient central pattern
S11	ZAP-70 tandem SH2-GFP	6	Transient central pattern
S12	PI3K tandem SH2-GFP	3	Diffuse (e.g. 3, 4) to central patterning
S13	SAP-GFP	4, 12	No patterning (2 x)
S14	Tec PH-TH-SH3-GFP	6	Rapid and highly transient central pattern
S15	Itk PH-TH-SH3-SH2-GFP	4, 5	Central to diffuse pattern (2 x)
S16	PLC-γ PH-SH2-SH2-GFP	4 (top)	Lamellal (e.g. 4) to central pattern
		4 (bottom)	Lamellal (e.g. 4, 5) to central pattern
S17	PKCη-GFP	7	Mostly diffuse pattern
S18	GFP-Cin85	5	Lamellal (e.g. 5, 8 – 10) to diffuse (e.g. 20) pattern
S19	GFP-CD2AP	5	Lamellal (e.g. 5, 6) to central pattern (37)
		24	Lamellal (e.g. 24 – 31) to various patterns
S20	GFP-PIP5K γ87	6	Various peripheral patterns (e.g. 6, 9, 15)
S21	GFP-PLC-δ PH	6	Transient distal (e.g. 6) and lamellal patterns (e.g. 8 – 10)
S22	GFP-Cytohesin PH	4	Weak and transient interface accumulation
S23	Rac sensor	24	Predominantly early central pattern
S24	Rho sensor	7	Transient invagination (8 – 11) to various patterning
S25	Arf6 sensor	4	MTOC-associated accumulation
S26	WAVE2-GFP	Preformed	Diffuse and peripheral patterns
		4	Diffuse and peripheral (e.g. 5, 15, 17, 19) patterns
S27	NFAT-GFP	8	Rapid cytoplasmic to nuclear translocation

Table S2. Numbers of cell couples analyzed. For each experimental condition, the number of cell couples analyzed is provided.

T cell APC Condition	5C.C7 CH27	5C.C7 DC	5C.C7 CH27 anti-B7	5C.C7 CH27 anti- ICAM	5C.C7 CH27 1/100 agonist	DO11.10 A20	OT II DC2.4
Receptors							
TCRζ	45					68	47
TCRζ 1-6	60						
TCRζ 1,2	52						
CD3ε	52						
I-Ek	75		41				
B7	49						
CD48	86						
ICAM-1	57						
Ly108-1	55						
CXCR4	59						
Cytoskeleton							
Actin	47		33	42	35	71	47
Tubulin	53						
Signaling intermediates							
ZAP-70	45					62	53
LAT	51						
SAP	56						
PI 3-kinase	56						
Tec	71						
Itk	30						
PLC γ	54						
Cin85	50					54	35
CD2AP	49						
PKC Θ	111	41	40	38	33	64	37
PI 5-kinase gamma 87	36						
PIP2	59						
PIP3	51						
Cdc42	27		44	44	43	66	45
Rac1	42		48	69	46		
RhoA	32						
Arf6	37						
WAVE2	24						
PKC η	76						
Transcription factor							
NFAT	52						
n exp	58						
n cell couples	2945						
avg	50.8						

References

1. N. S. van Oers, B. Tohlen, B. Malissen, C. R. Moomaw, S. Afendis, C. A. Slaughter, The 21- and 23-kD forms of TCR zeta are generated by specific ITAM phosphorylations. *Nat. Immunol.* **1,** 322–328 (2000).
2. K. Singelton, N. Parvaze, K. R. Dama, K. S. Chen, P. Jennings, B. Purtic, M. D. Sjaastad, C. Gilpin, M. M. Davis, C. Wülfing, A large T cell invagination with CD2 enrichment resets receptor engagement in the immunological synapse. *J. Immunol.* **177,** 4402–4413 (2006).
3. A. Borroto, D. Gil, P. Delgado, M. Vicente-Manzanares, A. Alcover, F. Sanchez-Madrid, B. Alarcon, Rho regulates T cell receptor ITAM-induced lymphocyte spreading in an integrin-independent manner. *Eur J Immunol* **30,** 3403–3410 (2000).
4. D. G. Woodside, D. K. Wooten, T. K. Teague, Y. J. Miyamoto, E. G. Caudell, T. Udagawa, B. F. Andruss, B. W. McIntyre, Control of T lymphocyte morphology by the GTPase Rho. *BMC Cell Biol* **4,** 2 (2003).
5. C. Wülfing, C. Sumen, M. D. Sjaastad, L. C. Wu, M. L. Dustin, M. M. Davis, Costimulation and endogenous MHC ligands contribute to T cell recognition. *Nat. Immunol.* **3**, 42–47 (2002).
6. I. Tskvitaria-Fuller, A. Seth, N. Mistry, H. Gu, M. K. Rosen, C. Wülfing, Specific patterns of Cdc42 activity are related to distinct elements of T cell polarization. *J. Immunol.* **177**, 1708–1720 (2006).
7. I. Tskvitaria-Fuller, A. L. Rozelle, H. L. Yin, C. Wulfing, Regulation of sustained actin dynamics by the TCR and costimulation as a mechanism of receptor localization. *J. Immunol.* **171**, 2287–2295 (2003).